Andreev Reflection and Cyclotron Motion of a Quasiparticle in High Magnetic Fields

Yasuhiro Asano[*] and Taichiro Kato

Department of Applied Physics, Hokkaido University, Sapporo 060-8628

We discuss the magnetoconductance oscillations in small junctions of a ballistic semiconductor and a superconductor. The conductance is calculated both numerically and analytically based on the Bogoliubov-de Gennes equation. The conductance oscillations appear when the Andreev reflection is not perfect at the interface and the diameter of the cyclotron motion of a quasiparticle is comparable to the width of the junction. An interplay between the cyclotron motion of a quasiparticle near the interface and the phase shift by the magnetic field is the origin of the conductance oscillations.

KEYWORDS: Andreev reflection, cyclotron motion, conductance oscillations, Aharonov-Bohm effect, Bogoliubov-de gennes equation

§1. Introduction

Magnetoconductance oscillations of a small ring are a one of fundamental consequence of the phase-coherent transport.[1] An electron wave traveling along one arm acquire a phase change, and an electron wave in the other arm suffer a different phase change because of the magnetic field. The conductance oscillates as a function of the magnetic flux encircled by a pair of electron waves traveling the different arms. The width of the arms must be narrow so that the number of the propagation path of an electron wave can be limited. If many propagation paths are allowed in the arms, the conductance oscillations are washed out. In order to observe the conductance oscillations clearly, at least, we have to either confine an electron wave as in the experiment[1] or the magnetic flux as in the original idea.[2] An electron wave, however, is confined within the cyclotron orbit by its charge degree of freedom under sufficiently strong magnetic fields, which is called the magnetic focusing.[3,4] In ballistic transport regime, it may be possible to observe the conductance oscillations without any artificial confinement of the electron wave and/or the magnetic flux. In this paper, we discuss the Aharonov-Bohm type conductance oscillations in a simply connected system.[5]

In recent years, study of small hybrid systems consisting of a superconductor in contact with a semiconductor has attracted much attention.[6-10] The unusual reflection from the normal metal-superconductor interface, known as the Andreev reflection,[11,12] characterizes the transport properties in semiconductor-superconductor (Sm-S) systems. In recent experiments, S-Sm-S junctions are realized in the strong magnetic fields by using a high H_{c2} superconductor.[13,14] The Josephson current is a consequence of the Andreev reflection at each Sm-S interface and is carried by the edge states in high magnetic fields.[15,16] Thus the Andreev reflection in the presense

of the magnetic field is one of the important topics in the mesoscopic Sm-S and S-Sm-S systems.

In this paper, we discuss the magnetoconductance oscillations in small Sm-S junctions, where a normal conduction occurs on high mobility two dimensional electron gas (2DEG) in a semiconductor. In real Sm-S junctions, the normal reflection is caused by several origins, such as the potential barrier at the Sm-S interface, the mismatch of the Fermi velocity on each side of the junction. In such situation, it is numerically shown that the sinusoidal oscillations appear in the magnetoconductance.[17] The authour mentioned that the conductance oscillations are similar to the Shubnikov-de Haas oscillations.[17] The mechanism, however, was not argued. We have revealed the nature of these novel magnetoconductance oscillations.[18] An interplay between the cyclotron motion of a quasiparticle and the phase shift by the magnetic field is responsible for the conductance oscillations in ballistic Sm-S junctions. The magnetoconductance oscillations are one of the interference effect of a quasiparticle and can be interpreted as the Aharonov-Bohm type effect in simply connected systems. In this paper, we show the detail of the numerical method and discuss the mechanism of the conductance oscillations in a phenomenological way. The amplitude and the period of the conductance oscillations are obtained analytically and show a good agreement with the numerical results. We also discuss the conditions to observe the conductance oscillations in experiments.

This paper is organized as follows. In §2, we explain the theoretical model and the method to calculate the conductance. The numerical results are shown in §3. The mechanism of the conductance oscillations is discussed and the analytic expression of the conductance is derived phenomenologically in §4. We discuss a possibility of observing the conductance oscillations in experiments in §5. The conclusion is given in §6. In Appendix, we derive the S-matrix of the one-dimensional Sm-S junctions.

---

* E-mail: asano@eng.hokudai.ac.jp

§2. Conductance of Sm-S Junctions

Let us consider a two-dimensional wire where electrons are confined in the y direction in the range of $-W/2 < y < W/2$. The wire consists of a 2DEG ($x < 0$) and a superconductor ($x > 0$) as shown in Fig. 1. The Sm-S junctions are described by the Bogoliubov-de Gennes equation[19]

$$\begin{pmatrix} H_0 & \Delta(x,y) \\ \Delta(x,y)^* & -H_0^* \end{pmatrix} \begin{pmatrix} u \\ v \end{pmatrix} = E \begin{pmatrix} u \\ v \end{pmatrix}, \quad (2.1)$$

where $u(x,y)$ and $v(x,y)$ are the wavefunctions of a quasiparticle. The Hamiltonian is given by

$$H_0 = -\frac{\hbar^2}{2m^*}\left\{\nabla - \frac{ie\boldsymbol{A}(x,y)}{\hbar c}\right\}^2 + U(x,y) - \mu, \quad (2.2)$$

where the effective mass of an electron m^* is m_N for $x \leq 0$ and m_S for $x > 0$, respectively. The chemical potential of the junction is denoted by μ. In what follows we set the chemical potential as an origin of the energy, i.e., $\mu = 0$. The Fermi energy in the 2DEG is μ_N which corresponds to the energy difference between the band edge and the chemical potential as shown in Fig. 1, where we schematically illustrate the dispersion relation on each side of the Sm-S junction in the absence of the magnetic field. The subband structure can be seen because of the confinement potential in the y direction. The Fermi energy in the superconductor is μ_S. The scalar potential $U(x,y)$ involves the hard wall confinement potential in the y direction and the potential barrier at the Sm-S interface which is described by $H\delta(x)$. The potential barrier height should be determined consistently by the electronic structure on each side of the junction.[20] In this paper, however, we treat H as one of the independent parameters of the Sm-S junctions. We assume that pair potential $\Delta(x,y)$ is Δ_0 in the superconductor and zero in the semiconductor, respectively. This model is justified when the superconducting segment is magnetically shielded. It is possible to realize this situation, for instance, by covering the superconducting segment with materials with high magnetic permeability. Here we assume that the superconductor is the type I. Since the magnetic field is not applied onto the superconductor, the vector potential is $\boldsymbol{A} = (0,0)$ for $x \geq 0$. The vector potential in the 2DEG ($x < 0$) is $\boldsymbol{A} = (0,Bx)$. In this model, we do not consider the self-consistency in the amplitude of the pair potential. In what follows, we measure the energy and the length in units of μ_N and $1/k_F \equiv \hbar/\sqrt{2m_N\mu_N}$, respectively.

In the semiconductor, the electronlike and the holelike excitations are decoupled because the pair potential is zero. When an electronlike quasiparticle is injected into the Sm-S interface from the nth propagating channel, the wavefunction in the 2DEG is given by

$$\hat{\Psi}_n^N(x,y) = \begin{pmatrix} 1 \\ 0 \end{pmatrix} e^{ik_n^+ x} f_n(y) \exp\left(i\frac{eB}{\hbar c}xy\right)$$
$$+ \sum_l A_{l,n} \begin{pmatrix} 1 \\ 0 \end{pmatrix} e^{-ik_l^+ x} g_l(y) \exp\left(i\frac{eB}{\hbar c}xy\right)$$
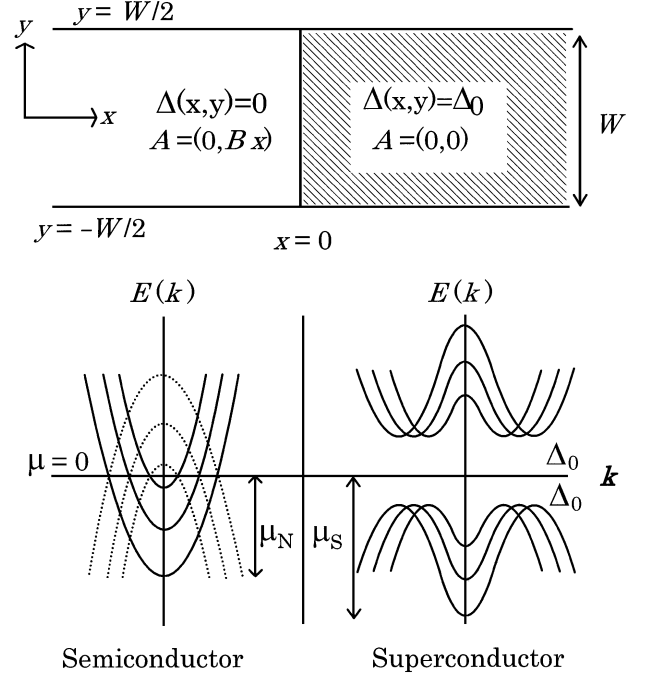

Fig. 1. The system under consideration is depicted in the upper figure. The Sm-S interface is at $x = 0$. In the y direction, an electron is confined in the range of $-W/2 < y < W/2$ by the hard wall potential. The dispersion relation on each side of the junction in an absence of the magnetic field are illustrated in the lower figure.

$$+ \sum_l B_{l,n} \begin{pmatrix} 0 \\ 1 \end{pmatrix} e^{ik_l^- x} h_l(y) \exp\left(-i\frac{eB}{\hbar c}xy\right), \quad (2.3)$$

where $A_{l,n}$ ($B_{l,n}$) is the reflection amplitude from the nth propagating channel in the electron branch to the lth channel in the electron (hole) branch. In the absence of the magnetic field, the wavefunction in the y direction and the wavenumber in the lth channel are given by

$$\chi_l(y) = \sqrt{\frac{2}{W}} \sin\left\{\frac{l\pi}{W}\left(y + \frac{W}{2}\right)\right\}, \quad (2.4)$$

$$k_l^\pm = \sqrt{\frac{2m_N(\mu_N \pm E)}{\hbar^2} - \left(\frac{l\pi}{W}\right)^2}, \quad (2.5)$$

where k^+ and k^- represent the wavenumber of the electronlike and holelike excitations, respectively. In the presence of the magnetic field, the wavefunction in the y direction, $f_n(y)$, $g_l(y)$ and $h_l(y)$, are described by the linear combination of $\chi_l(y)$'s. Here we first compute the wavefunction in magnetic field under the vector potential $\boldsymbol{A} = (-By,0)$ by using a numerical method.[21] Then we apply the gauge transformation from $\boldsymbol{A} = (-By,0)$ to $(0,Bx)$. The phase factor in eq. (2.3) stems from the gauge transformation.

In the superconductor, the wavefunction is

$$\hat{\Psi}_n^S(x,y) = \sum_l C_{l,n} \begin{pmatrix} u_0 \\ v_0 \end{pmatrix} e^{iq_l^+ x} \chi_l(y)$$
$$+ \sum_l D_{l,n} \begin{pmatrix} v_0 \\ u_0 \end{pmatrix} e^{-iq_l^- x} \chi_l(y), \quad (2.6)$$

where the wavenumber of a quasiparticle satisfies the equation

$$\frac{\hbar^2 q_l^{\pm 2}}{2m_S} = \mu_S - \frac{\hbar^2}{2m_S}\left(\frac{l\pi}{W}\right)^2 \pm \sqrt{E^2 - \Delta_0^2}, \qquad (2.7)$$

for $E > \Delta_0$ and

$$\frac{\hbar^2 q_l^{\pm 2}}{2m_S} = \mu_S - \frac{\hbar^2}{2m_S}\left(\frac{l\pi}{W}\right)^2 \pm i\sqrt{\Delta_0^2 - E^2}, \qquad (2.8)$$

for $E < \Delta_0$, respectively. The coefficients $C_{l,n}$ and $D_{l,n}$ are transmission amplitude from nth propagating channel in the 2DEG to the lth channel in the superconductor. The amplitudes of the wavefunction are given by

$$u_0 = 1/\sqrt{2}, \qquad (2.9)$$

$$v_0 = \frac{E - i\sqrt{\Delta_0^2 - E^2}}{\sqrt{2}\Delta_0}, \qquad (2.10)$$

for $E < \Delta_0$ and

$$u_0^2 = \frac{1}{2}\left(1 + \frac{\sqrt{E^2 - \Delta_0^2}}{E}\right), \qquad (2.11)$$

$$v_0^2 = \frac{1}{2}\left(1 - \frac{\sqrt{E^2 - \Delta_0^2}}{E}\right), \qquad (2.12)$$

for $E > \Delta_0$, respectively. The amplitudes, $A_{l,n}$, $B_{l,n}$, $C_{l,n}$ and $D_{l,n}$, are determined by the continuity condition of the wavefunction at $x = 0$,

$$\left[\hat{\Psi}_n^N - \hat{\Psi}_n^S\right]\Big|_{x=0} = 0, \qquad (2.13)$$

$$\frac{d}{dx}\left[\hat{\Psi}_n^N - \frac{m_N}{m_S}\hat{\Psi}_n^S\right]\Big|_{x=0} = -\frac{2m_N H}{\hbar^2}\hat{\Psi}_n^S\Big|_{x=0}. \qquad (2.14)$$

From the amplitudes, $A_{l,n}$ and $B_{l,n}$, we can calculate the reflection probability as

$$R_{l,n}^{ee}(E) = |v_l^+/v_n^+| \, |A_{l,n}|^2, \qquad (2.15)$$

$$R_{l,n}^{he}(E) = |v_l^-/v_n^+| \, |B_{l,n}|^2, \qquad (2.16)$$

where $v_l^{+(-)}$ is the velocity in the lth propagating channel in the electron (hole) branch. At the zero temperature, the differential conductance is given by

$$G(eV) = \frac{2e^2}{h}\sum_{l,n}'\left(\delta_{l,n} - R_{l,n}^{ee} + R_{l,n}^{he}\right), \qquad (2.17)$$

with $E = eV$,[22] where the summation $\sum' = N_c$ runs over the all propagating channels in the 2DEG under the magnetic field and V is the bias voltage. When $E = eV < \Delta_0$, there is no propagating channel in the superconductor. Thus the current conservation low implies

$$\sum_l'\left(R_{l,n}^{ee} + R_{l,n}^{he}\right) = 1. \qquad (2.18)$$

§3. Numerical Results

In Fig. 2, we show the numerical results of the zero-bias differential conductance ($eV \to 0$) in units of $2e^2/h$ as a function of $\mu_N/\hbar\omega_c$, where $\omega_c = eB/cm_N$ and $\Delta_0/\mu_N = 0.02$, respectively. Since the pair potential in a
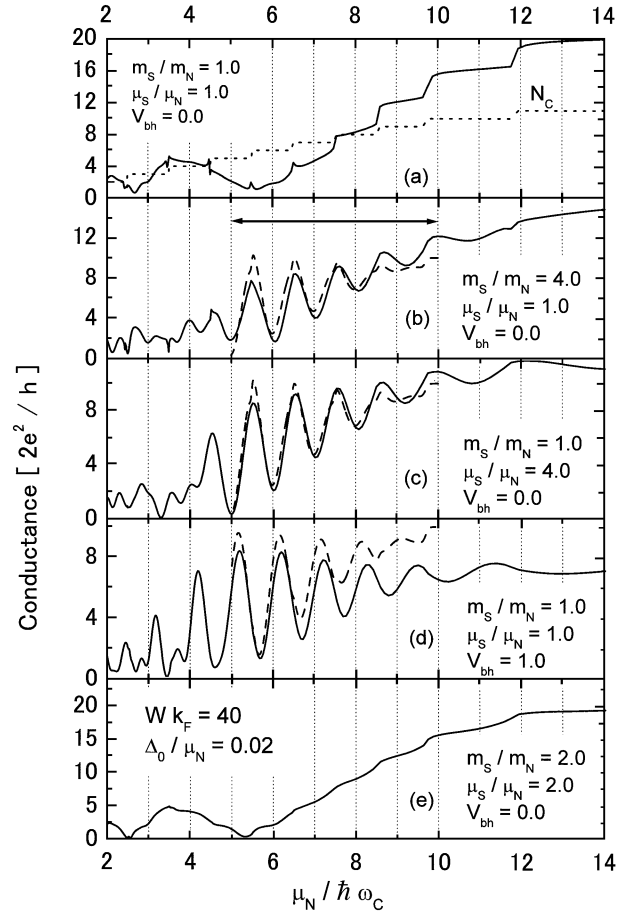

Fig. 2. The conductance is numerically calculated as a function of the inverse of the magnetic field. Here the width of the wire and the pair potential are fixed at $Wk_F = 40$ and $\Delta_0/\mu_N = 0.02$, respectively. The number of the propagating channels in 2DEG is plotted by a dash line in (a). In (a) and (e), the normal reflection at the Sm-S interface is negligible. On the other hand, the normal reflection occurs at the interface and the conductance oscillations appear in (b), (c) and (d). We compare the analytic expression of the conductance (dash line) with the numerical results in (b)-(d). The range of the magnetic fields which satisfy $W/2 < L_c < W$ is denoted by $\leftrightarrow$ in (b).

superconductor is typically 1 meV and the Fermi energy in a semiconductor is about 100 meV, we fix Δ_0/μ_N at 0.02 throughout this paper. Here we fix the width of the wire Wk_F at 40. The numerical results here are essentially the same with those in the previous paper.[17] We consider the ratio of the effective mass and the potential barrier at the Sm-S interface in addition to the ratio of the Fermi energy. There are three parameters which characterize the transparency of the Sm-S junctions: (i) the ratio of the Fermi energy, μ_S/μ_N, (ii) the ratio of the effective mass, m_S/m_N, and (iii) the potential barrier at the Sm-S interface, $V_{bh} \equiv 2m_N H/\hbar^2 k_F$. In Fig. 2(a), we show the results for $\mu_S/\mu_N = 1.0$, $m_S/m_N = 1.0$ and $V_{bh} = 0.0$, where we do not consider the difference of the effective mass, the difference of the Fermi energy nor the potential barrier at the interface. The results show the conductance step for $\mu_N/\hbar\omega_c > 5$ and the conductance decreases with increasing the magnetic field. In this case, we confirm that the normal reflection does not occur at the interface from numerical data, i.e., $R_{l,n}^{ee} \simeq 0$. This can be also understood by the S-matrix in the one-

dimensional Sm-S junctions given by eqs. (A·14)–(A·22) in the Appendix. In the present situation, $\xi = 1$ leads to $r_{ee} = 0$. With using eq. (2.18), the conductance results in $G = 4e^2/h \sum_l '$. The conductance is changed by $4e^2/h$ when one of the propagating channels is depopulated by the magnetic field. In Fig. 2(a), the number of the propagating channels in the 2DEG, N_c, is plotted with the dot line. For $\mu_N/\hbar\omega_c < 6$, the oscillatory behavior can be seen in the conductance. These oscillations appear only when the Andreev reflection is perfect and are periodic as a function of $\hbar\omega_c/\mu_N$.[17]

Next we consider the difference of the effective mass in Fig. 2(b) and the difference of the Fermi energy in Fig. 2(c), where $\mu_S/\mu_N = 1.0$, $m_S/m_N = 4.0$ and $V_{bh} = 0.0$ in (b) and $\mu_S/\mu_N = 4.0$, $m_S/m_N = 1.0$ and $V_{bh} = 0.0$ in (c), respectively. The results show the sinusoidal conductance oscillations and the conductance is at its minimum when $\mu_N/\hbar\omega_c$ is an integer. In the presence of the mismatch in the effective mass or that in the Fermi energy, the Andreev reflection is no longer perfect, which can be also described by the S-matrix in one-dimensional Sm-S junctions, i.e., $\xi \neq 1$. In Fig. 2(d), we exiamine the effects of the potential barrier at the interface, where $\mu_S/\mu_N = 1.0$, $m_S/m_N = 1.0$ and $V_{bh} = 1.0$. The results show the conductance oscillations as well as those in (b) and (c). Here we note the fact that the conductance does not take its minimum when $\mu_N/\hbar\omega_c$ is an integer. The potential barrier causes the phase shift in the conductance oscillations. The author of the previous paper[17] has been pointing out a similarity between the conductance oscillations and the Shubnikov-de Haas oscillations because the conductance takes its maximum when one of the propagating channel in 2DEG is magnetically depopulated. Their suggestion, however, is not true since the maxima in the conductance are shifted by introducing the potential barrier at the interface. In addition, there is no disorder in the present system.

As shown in eqs. (A·14)–(A·22), the normal reflection is expected to be zero in one-dimensional Sm-S junctions when $\mu_S/\mu_N = m_S/m_N$ and $V_{bh} = 0$. The situation is almost the same even in the two-dimensional junctions under the magnetic field. We show the conductance for $\mu_S/\mu_N = m_S/m_N = 2.0$ in Fig. 2(e), where $V_{bh} = 0.0$. The sinusoidal oscillations disappear and the weak conductance step again can be seen as well as in Fig. 2(a). Thus we conclude that the magnetoconductance oscillates when both the normal and the Andreev reflection occur at the Sm-S interface irrespective of the origin of the normal reflection. We should note that the S-matrix in the one-dimensional junctions well describes the characteristic feature of the Andreev reflection probability in the two-dimensional systems although the dimensionality in the two systems are different. One explanation for this is as follows. The amplitudes of the normal and the Andreev reflections are determined by the microscopic parameters, such as μ_S/μ_N, m_S/m_N and V_{bh}. These parameters, however, do not include the dimensionality explicitly in our simple model.

In Fig. 3, we show the zero-bias conductance for several choices of the width of the wire, where $\mu_S/\mu_N = 4.0$, $m_S/m_N = 1.0$ and $V_{bh} = 0.5$. The width of the wire is
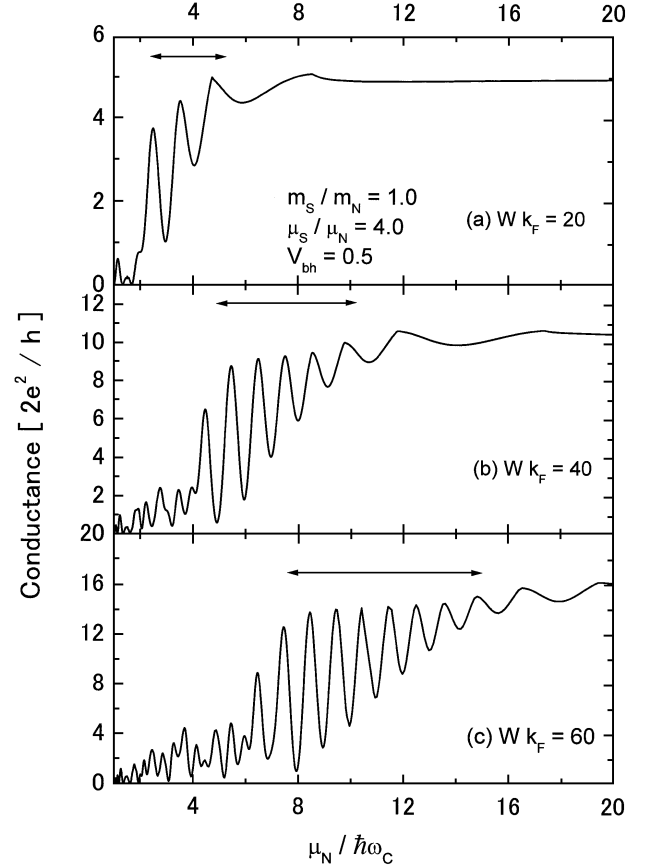

Fig. 3. The conductance is numerically calculated as a function of the inverse of the magnetic field for several choices of the with of wire, where $Wk_F = 20$, 40 and 60 in (a), (b) and (c), respectively. The range of the magnetic fields which satisfy $W/2 < L_c < W$ is denoted by $\leftrightarrow$.

$Wk_F = 20$, 40 and 60 in Figs. 3(a), 3(b) and 3(c), respectively. The conductance oscillates as a function of the magnetic field because both the normal and the Andreev reflection occur at the interface in the present situation. The range of the magnetic fields in which the oscillations can be seen shifts to the higher region of $\mu_N/\hbar\omega_c$ with increasing W. The range of the magnetic fields which satisfy the equation

$$\frac{W}{2} < L_c < W, \tag{3.1}$$

$$L_c \equiv \frac{4}{k_F}\frac{\mu_N}{\hbar\omega_c}, \tag{3.2}$$

is denoted by $\leftrightarrow$ in Figs. 3 and 2(b). Here L_c is the diameter of the classical cyclotron motion of a quasiparticle in the 2DEG. The results show that the conductance oscillations appear when the magnetic field is satisfying eq. (3.1), which indicates that the cyclotron motion of a quasiparticle plays an important role in the conductance oscillations. We calculate the amplitude of the wavefunction which is reflected into the electron and hole branches as shown in Fig. 4. Here we focus on the system shown in Fig. 3(b) and fix the magnetic field at $\mu_N/\hbar\omega_c = 8.0$. The amplitudes of the wavefunction are defined by
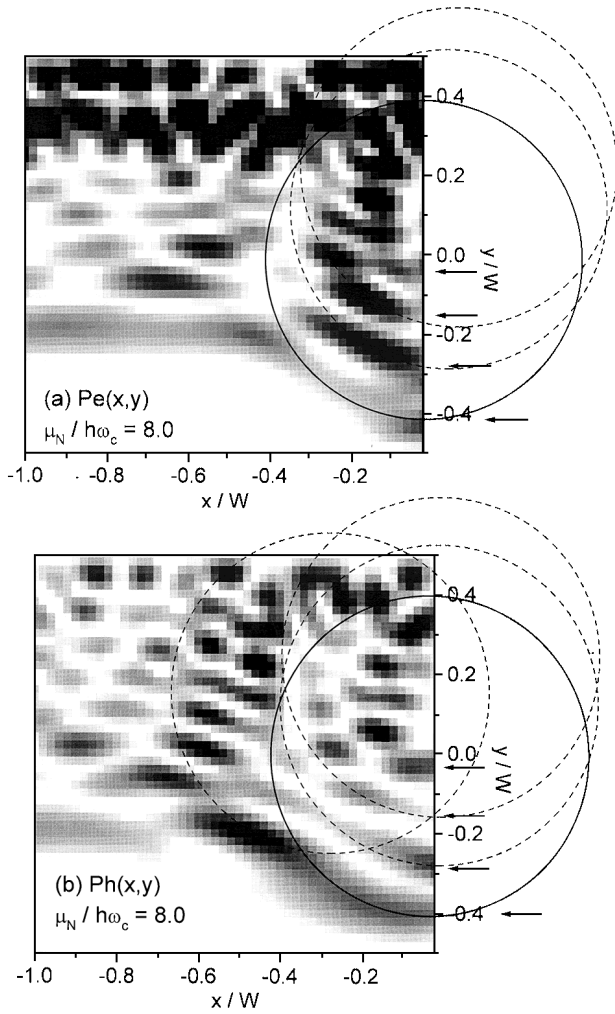
Fig. 4.   The amplitudes of the wavefunction reflected into the electron (a) and hole (b) branches are shown, where $Wk_F = 40$, $\Delta_0/\mu_N = 0.02$, $m_S/m_N = 1.0$ and $\mu_S/\mu_N = 4.0$, $V_{bh} = 0.5$, respectively. We fix the magnetic field at $\mu_N/\hbar\omega_c = 8.0$. The classical trajectory of a cyclotron motion is represented by the circles.

$$P_e(x,y) = \left| {\sum_n}' \sum_l A_{l,n} e^{-ik_l^+ x} g_l(y) \right|^2 , \qquad (3.3)$$

$$P_h(x,y) = \left| {\sum_n}' \sum_l B_{l,n} e^{ik_l^- x} h_l(y) \right|^2 , \qquad (3.4)$$

and are represented in Figs. 4(a) and 4(b), respectively. In the dark area, $P_{e(h)}(x,y)$ has the large amplitudes. An electronlike quasiparticle is injected from the lower left corner. It is important that an incident wave does not have uniform amplitudes at the Sm-S interface but has the large amplitudes at several points, such as $y/W \sim -0.4, -0.26, -0.13$ and -0.005 as indicated by the arrows. The classical trajectories of the cyclotron motion of a quasiparticle are represented by the circles which are drawn to fit the interference pattern for $y < 0$ and to pass the reflection points at the interface. It is possible to draw another circles in the figure. We omit them to avoid complexity. The amplitudes of the wavefunction seems to be characterized well by the cyclotron orbits for $y < 0$. For $0 < y$, however, it is difficult to find the classical trajectories because of the interference effect.
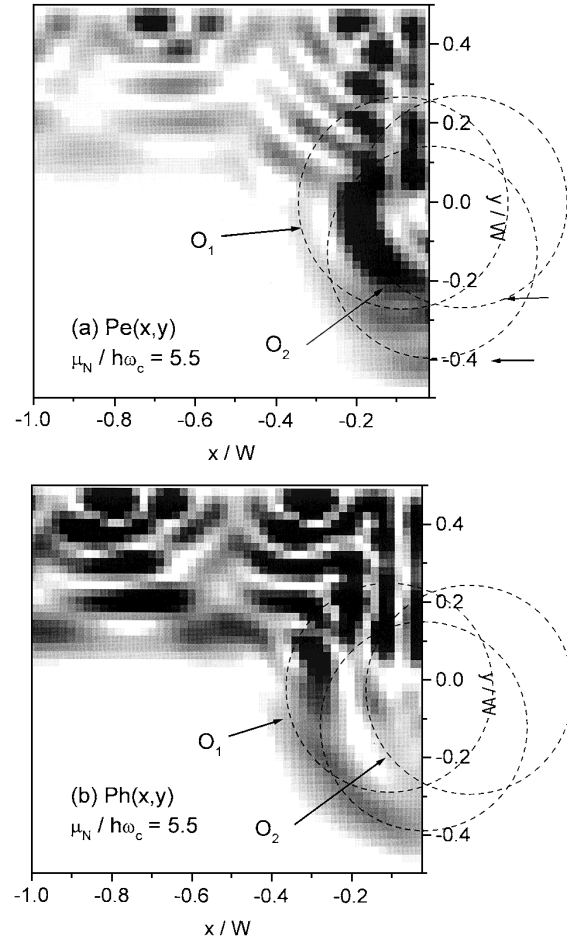

Fig. 5.   The amplitudes of the wavefunction reflected into the electron (a) and hole (b) branches are shown, where we fix the magnetic field at $\mu_N/\hbar\omega_c = 5.5$.

Under the magnetic field, an electron localizing near the edge of the wire has the larger velocity in the x direction than that localizing around the center of the wire. Thus at $y/W = -0.4$, the wave is reflected almost perpendicular to the interface, which corresponds to the fact that the lowest circle is symmetric about $x = 0$. The waves at another reflection points have the momentum in the y direction, which allows the asymmetric circles about $x = 0$. The amplitude in the electron branch at the upper left corner is much larger than that in the hole branch, which reflects the fact that the conductance is around its minimum at $\mu_N/\hbar\omega_c = 8.0$ as shown in Fig. 3(b). In Fig. 5, we show the amplitudes of a quasiparticle at the higher magnetic field, where $\mu_N/\hbar\omega_c = 5.5$. At the Sm-S interface, an incident quasiparticle has the large amplitudes around $y/W = -0.4$ and -0.28 as indicated by the two arrows. The circle passing $y/W = -0.4$ seems to be symmetric about $x = 0$ because the velocity in the x direction is much larger than that in the y direction. At $y/W = -0.28$, it may be possible to draw two circles, which are symmetric with each other about $x = 0$. At the upper left corner, the amplitude in the electron branch is much smaller than that in the hole branch, which reflects the fact that the conductance is around one of its maxima at $\mu_N/\hbar\omega_c = 5.5$ as shown in Fig. 3(b). In upper left corner, several skipping orbits running away from the interface can be seen clearly. The

results show that the motion of a quasiparticle is characterized well by the classical cyclotron orbits near the Sm-S interface. We note that the concept of the classical cyclotron motion is not valid in quite strong magnetic fields $\mu_N/\hbar\omega_c < 1$ where the magnetic length, $\sqrt{\hbar c/eB}$, is comparable to L_c.

Before turning into the phenomenological analysis, we summarize the characteristic feature of the magnetoconductance oscillations. (i) The oscillations appear when the both the normal and Andreev reflection occur at the interface. (ii) The conductance oscillates periodically as a function of the inverse of the magnetic field. (iii) The potential barrier at the interface causes the phase shift in the conductance oscillations. (iv) The oscillations appear when the magnetic fields satisfy eq. (3.1).

§4. Mechanism of the Conductance Oscillations

In the range of the magnetic fields described by eq. (3.1), an incident quasiparticle from the electron branch on the semiconductor side can be scattered twice at the Sm-S interface as shown in Fig. 6. At first an incident electron is either reflected into the electron branch by the normal reflection or the hole branch by the Andreev reflection. In the presence of the magnetic field, the trajectories of the reflected wave are characterized by the cyclotron orbits. After the ballistic cyclotron motion, the quasiparticle in each branch is reflected again into the electron and hole branches. After suffering the two reflections at the Sm-S interface, an incident electron divides into four parts as shown in Fig. 6. In Figs. 6(a) and 6(c) (Figs. 6(b) and 6(d)) an incident quasiparticle is first reflected into the electron (hole) branch at $\boldsymbol{r}_1$. Then in Figs. 6(a) and 6(b) (Figs. 6(c) and 6(d)) a quasiparticle is reflected into the electron (hole) branch at $\boldsymbol{r}_2$. The phase of a quasiparticle is changed by the magnetic field while traveling along the cyclotron orbit near the interface. When a quasiparticle is in the electron branch, the phase shift due to the magnetic field can be calculated as

$$\phi_B = \frac{e}{\hbar c} \int_{\boldsymbol{r}_1}^{\boldsymbol{r}_2} \mathrm{d}\boldsymbol{r}_N \cdot \boldsymbol{A}(\boldsymbol{r}_N) = -\pi\frac{\mu_N}{\hbar\omega_c}, \qquad (4.1)$$

where $\boldsymbol{r}_N$ is the integration path along the cyclotron orbit between $\boldsymbol{r}_1$ and $\boldsymbol{r}_2$. On the other hand, the phase change of a quasiparticle in the hole branch is given by $-\phi_B$ because the sign of the charge in the holelike excitation is opposite to that in the electronlike excitation. In the following, we separate the scattering process into three process. We describe the two reflections at the Sm-S interface by using the S-matrix in one-dimensional junctions which is given in the Appendix. The effects of the two-dimensionality and those of the magnetic field are taken into account through the phase shift which should be multiplied to the wavefunction while traveling across the wire along the cyclotron orbit. In this way, we phenomenologically estimate the wavefunction of the four parts as follows,

$$\Psi_1^e = |r_{ee}|\mathrm{e}^{\mathrm{i}\theta_n} \cdot \mathrm{e}^{\mathrm{i}\phi_B} \cdot |r_{ee}|\mathrm{e}^{\mathrm{i}\theta_n}, \qquad (4.2)$$

$$\Psi_2^e = |r_{eh}|\mathrm{e}^{-\mathrm{i}\pi/2} \cdot \mathrm{e}^{-\mathrm{i}\phi_B} \cdot |r_{he}|\mathrm{e}^{-\mathrm{i}\pi/2}, \qquad (4.3)$$
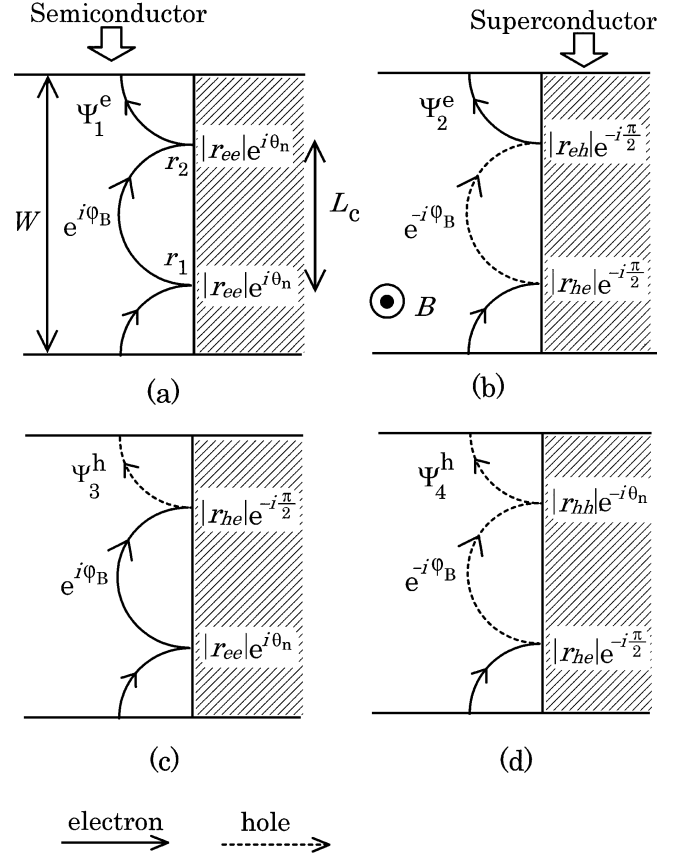

Fig. 6. Schematic picture of the reflection process from the Sm-S interface. The width of the junction is W and the diameter of the cyclotron motion is L_c. The shaded area represents the superconducting segment. The solid and broken lines denote a quasiparticle in the electron and hole branches, respectively.

$$\Psi_3^h = |r_{he}|\mathrm{e}^{-\mathrm{i}\pi/2} \cdot \mathrm{e}^{\mathrm{i}\phi_B} \cdot |r_{ee}|\mathrm{e}^{\mathrm{i}\theta_n}, \qquad (4.4)$$

$$\Psi_4^h = |r_{hh}|\mathrm{e}^{-\mathrm{i}\theta_n} \cdot \mathrm{e}^{-\mathrm{i}\phi_B} \cdot |r_{he}|\mathrm{e}^{-\mathrm{i}\pi/2}. \qquad (4.5)$$

In the analysis, we use relations $\Delta_0 \ll \mu_N$ and $E = 0$. The phase shift of the Andreev reflection is $-\pi/2$ and that of the normal reflection is θ_n. The two parts in the electron branch in eqs. (4.2) and (4.3) interfere with each other and $|\Psi_1^e + \Psi_2^e|^2$ represents the reflection probability into the electron branch. In the same way, $|\Psi_3^h + \Psi_4^h|^2$ is the reflection probability into the hole branch. The conductance is roughly estimated by

$$G \sim g_0 \left[1 - |\Psi_1^e + \Psi_2^e|^2 + |\Psi_3^h + \Psi_4^h|^2 \right] \qquad (4.6)$$

$$= g_0 \left[1 - \left(|r_{ee}|^2 - |r_{he}|^2 \right)^2 \right.$$

$$\left. + 4|r_{ee}|^2|r_{he}|^2 \cos\left(2\pi\frac{\mu_N}{\hbar\omega_c} - 2\theta_n \right) \right], \quad (4.7)$$

where $g_0 = 2e^2/h\sum_n{}'$. In real space, the cyclotron orbits of the two waves, for instance Ψ_1^e and Ψ_2^e, do not encircle the magnetic flux. However, the phase shift by the magnetic field in Ψ_1^e has the opposite sign to that in Ψ_2^e. This is because a quasiparticle traverses the wire in the electron branch in Ψ_1^e and in the hole branch in Ψ_2^e, respectively. This argument can be also applied to Ψ_3^h and Ψ_4^h. The magnetic field causes the interference effect and the conductance oscillates as a function of the magnetic
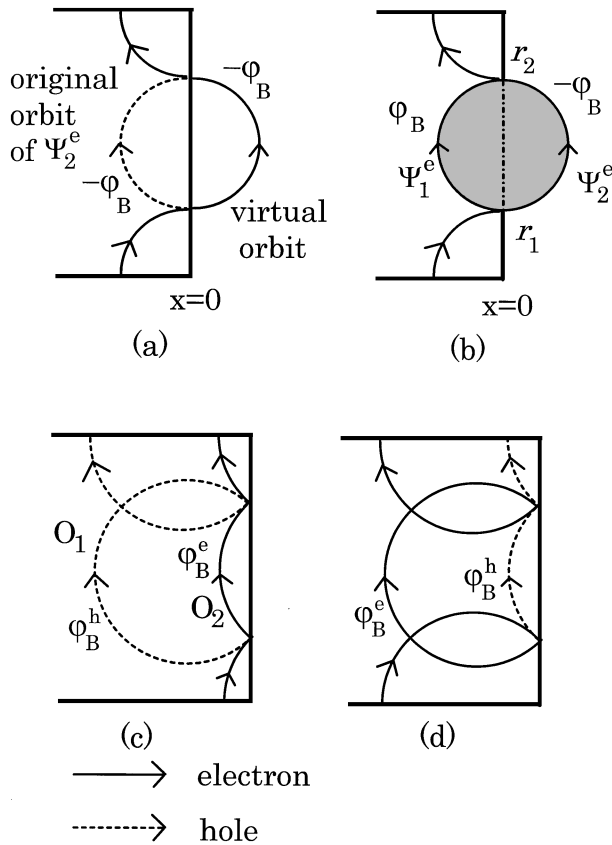
Fig. 7.   The phase shift along the original cyclotron orbit in the
hole branch is equal to that along the virtual cyclotron orbit in
the electron branch (a). The magnetic flux in gray region in units
of ϕ_0 is corresponding to $\mu_N/\hbar\omega_c$ in (b). The cyclotron orbits
of a quasiparticle whose incident angle is not perpendicular to
the Sm-S interface are depicted in (c) and (d). The two incident
waves in (c) and (d) are the source of the asymmetric orbits
about $x = 0$ in Fig. 5.

field. The mechanism of the interference effect in the
present system is analogous to the Aharonov-Bohm type
interference effect in a small ring.[1] Let us draw a virtual
cyclotron orbit on the right hand side of the junction as
shown in Fig. 7(a). Here we draw the virtual orbit in the
electron branch which corresponds to the original orbit in
the hole branch in Ψ_2^e. The virtual orbit must be drawn
to be symmetric with the original orbit about $x = 0$. The
phase shift along the original cyclotron orbit in the hole
branch is exactly equal to that along the virtual orbit in
the electron branch. An incident quasiparticle is sepa-
rated into two orbits at $\boldsymbol{r}_1$: one is the real cyclotron orbit
in Ψ_1^e (semi-circle on the left in Fig. 7(b)), the other is the
virtual orbit in Ψ_2^e (semi-circle on the right). These two
waves come across at $\boldsymbol{r}_2$ after suffering the different phase
shift. Thus the situation is almost equivalent to the small
ring in the experiment.[1] The magnetic flux in the gray
area in Fig. 7(b) in units of $\phi_0 = hc/e$ is correspond-
ing to $\mu_N/\hbar\omega_c$. The diameter of the cyclotron motion
L_c itself depends on the magnetic fields, the oscillations
become periodic as a function of the inverse of the mag-
netic field. In the absence of the potential barrier at the
Sm-S interface (i.e., $V_{bh} = 0$), θ_n becomes zero as shown
in eq. (A·22) and the conductance is at its maximum
when $\mu_N/\hbar\omega_c$ is an integer as shown in eq. (4.7). The

numerical results, however, show that the conductance
takes its minimum at $\mu_N/\hbar\omega_c$ is an integer. The sign of
the oscillating part is a disagreement between the simple
analysis and the numerical results. In our analysis, we
do not explicitly consider the two-dimensionality of the
system. The disagreement may stem from the wavefunc-
tion in the y direction. At present, we can not give a
satisfactory explanation of the disagreement within the
phenomenological argument. A recent microscopic cal-
culation may explain this point clearly.[23] The simple
analysis also explain the phase shift of the oscillations in
the presence of the potential barrier at the Sm-S interface
as shown in Fig. 2(d).

In Fig. 6, we assume that the motion of a quasiparticle
near the Sm-S interface is characterized by semi-circles
of the cyclotron orbit. For instance in Figs. 5(c) and
5(d), however, the asymmetric circles about $x = 0$ can
be seen (O_1 and O_2). Here we show that the asymmet-
ric orbits give the same contribution to the conductance
oscillations with the symmetric orbits. In Figs. 7(c)
and 7(d), we show the classical motion of a quasipar-
ticle whose incident angle is not perpendicular to the
interface. The cyclotron orbits O_1 and O_2 in Fig. 5 cor-
respond to those in Figs. 7(c) and 7(d). In Fig. 7(c),
a quasiparticle is injected to the interface with positive
velocity in the y direction and is scattered into the elec-
tron and hole branches. The reflected quasiparticle in
the electron branch travels along O_2, whereas the corre-
sponding part in the hole branch traverse the wire along
O_1. This is because only the velocity component perpen-
dicular to the interface changes sign in the normal reflec-
tion, however, all velocity components change sign in the
Andreev reflection.[11] The phase difference, $\phi_B^e - \phi_B^h$, is
equal to $2\phi_B$ independent of the incident angle. This can
be easily confirmed when we draw a virtual cyclotron or-
bit corresponding to O_1 on the right hand side of the
junction. The asymmetric cyclotron orbits, therefore,
can contribute to the conductance oscillations as well as
the symmetric orbits. From Figs. 7(c) and 7(d), it is pos-
sible to understand that the two incident wave (c) and
(d) do not interfere with each other. This is because the
cyclotron orbits of the outgoing wave in electron branch
in (c) is separated from that in (d) in space. The same
argument can be applied to the outgoing cyclotron or-
bits in the hole branch. Those feature of a quasiparticle
near the Sm-S interface are natural consequence of the
Andreev reflection in high magnetic fields. Thus we con-
clude that the Aharonov-Bohm type conductance oscilla-
tions can be seen even in the simply connected systems.
A possibility of the Aharonov-Bohm type conductance
oscillations was briefly mentioned.[17] A part of their ar-
gument, however, was incorrect, which leads to negative
conclusion.

When the magnetic field is weak as shown in Fig. 4,
only the orbit drawn with the solid circle can contribute
to the conductance oscillations. Along the solid circle,
a quasiparticle can return to the interface after the cy-
clotron motion. On the other hand, another orbits rep-
resented with the dash lines go across the wire wall at
$y/W = 0.5$ before reaching the interface. Thus such
orbits do not contribute to the conductance oscillations

and we have to neglect these orbits. When the magnetic field is relatively strong as shown in Fig. 5, most of the reflected wave can contribute to the conductance oscillations. The amplitude of the conductance oscillations is expected to be increase with increasing the magnetic field. The contribution ratio is roughly estimated as follows. We focus on the range of the magnetic fields in eq. (3.1). When $W/2 = L_c$, the contribution ratio is set to be unity. On the other hand, the contribution ratio may be zero at $W = L_c$. Thus we approximately describe the contribution ratio by using a linear function of $\mu_N/\hbar\omega_c$

$$p\left(\frac{\mu_N}{\hbar\omega_c}\right) = 2\left(1 - \frac{L_c}{W}\right) = 2\left(1 - \frac{4}{Wk_F}\frac{\mu_N}{\hbar\omega_c}\right). \quad (4.8)$$

The wavefunction in eqs. (4.2)–(4.5) should be multiplied by $p\left(\frac{\mu_N}{\hbar\omega_c}\right)$ and the conductance in eq. (4.7) should be rewriten as

$$G \sim g_0\left[1 + 4|r_{ee}|^2|r_{he}|^2 p\left(\frac{\mu_N}{\hbar\omega_c}\right)^2\right.$$
$$\left.\times \cos\left(2\pi\frac{\mu_N}{\hbar\omega_c} - 2\theta_n\right)\right]. \quad (4.9)$$

We have neglected $\left(|r_{ee}|^2 - |r_{he}|^2\right)^2$ because this is much smaller than unity when both the normal and Andreev reflection occur at the Sm-S interface. In Fig. 2, we compare eq. (4.9) (dash line) with the numerical results, where $|r_{ee}|$ and $|r_{he}|$ are calculated by using eqs. (A·14)–(A·22), and N_c is shown in Fig. 2(a) with the dash line. The results show an excellent agreement with each other. Here we have to confess that the sign of the second term in eq. (4.9) has been changed from $+$ to $-$ in Fig. 2. Except for the sign of the oscillating part, the analytical results in eq. (4.9) explain the characteristic behavior of the conductance oscillations which are summarized in the end of §3.

§5. Discussion

In Figs. 2 and 3, we have studied the zero-bias differential conductance. Here we show the results of the differential conductance at the finite bias voltage in Fig. 8, where $Wk_F = 40$, $\Delta_0/\mu_N = 0.02$, $\mu_S/\mu_N = 4.0$, $m_S/m_N = 1.0$ and $V_{bh} = 1.0$, respectively. The bias voltage are given by $eV/\Delta_0 = 0.5$ and 1.5, respectively. The conductance oscillations can be seen even at the finite bias voltage for $eV < \Delta_0$. The Fermi energy effectively increases (decreases) by eV for an electronlike (holelike) quasiparticle in the 2DEG. Consequently, the diameter of the cyclotron motion is slightly changed to $L_c(1+eV/\mu_N)$ in the electron branch and $L_c(1 - eV/\mu_N)$ in the hole branch, respectively. In the situation $eV < \Delta_0 << \mu_N$, however, the diameter of the cyclotron motion, therefore, the magnetic flux encircled by the cyclotron orbits almost remain unchanged. Thus the oscillations appear in the finite bias conductance for $eV < \Delta_0$. The oscillations disappear in the differential conductance at $eV/\Delta_0 = 1.5$ since the amplitude of the Andreev reflection decreases rapidly with increasing eV for $eV > \Delta_0$.[12] The results in Fig. 8 are consistent with the phenomenological argu-
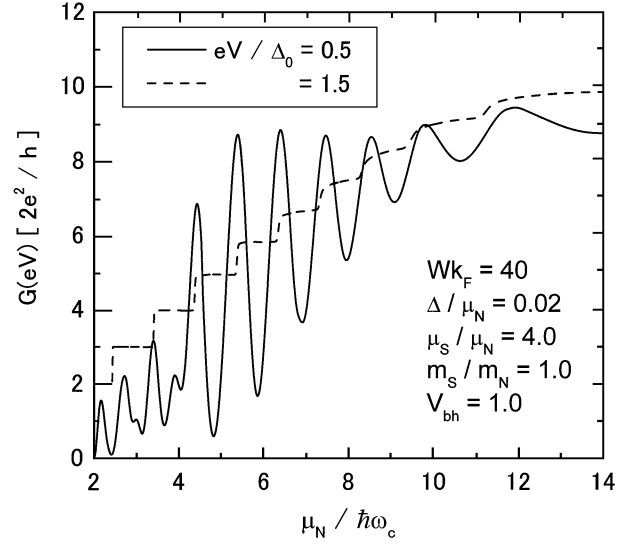

Fig. 8. The differential conductance at the finite bias voltage is plotted as a function of $\mu_N/\hbar\omega_c$, where $Wk_F = 40$, $\Delta_0/\mu_N = 0.02$, $\mu_S/\mu_N = 4.0$, $m_S/m_N = 1.0$ and $V_{bh} = 1.0$, respectively. The bias voltage is given by $eV/\Delta_0 = 0.5$ and 1.5.

ment.

When the width of the wire is $W = 5 \times 10^{-6}$ m as in a experiment,[13] the range of the magnetic fields given by eq. (3.1) can be estimated to be $B = 0.1 \sim 0.2$ T. We use the parameters such as $\mu_N = 100$ meV, $m_N/m_e = 0.05$, where m_e is the bare mass of an electron. We have neglected the Zeeman spin splitting in the 2DEG which can be taken into account in the same way with the exchange potential in ferromagnetic metals.[24] In the presence of the Zeeman splitting, the diameter of the cyclotron orbit in the electron (hole) branch is estimated to be $L_c(1+(-)g\mu_B B/2\mu_N)$, where g and μ_B are Lande's factor and Bohr magneton, respectively. The correction is also quite small in semiconductors such as InAs and GaAs when the magnetic field is smaller than 1 T.

The theoretical model used in this study is justified in a situation where the superconducting segment is magnetically shielded. We have not considered the phase fluctuations of the pair potential due to the magnetic field. When the magnetic screening is not perfect, the phase fluctuations may affect the conductance oscillations because a quasiparticle acquires the local phase of the pair potential at the Andreev reflection points. In such situation, the argument should be slightly modified. Let us assume that the phase of the pair potential at $\boldsymbol{r}_1$ and $\boldsymbol{r}_2$ in Fig. 6 are θ_1 and θ_2, respectively. In this case the oscillating part of the conductance in eq. (4.9) is modified to

$$\delta G \propto \cos\left(F + 2\theta_n\right), \quad (5.1)$$

$$F \equiv 2\phi_B + \theta_1 - \theta_2. \quad (5.2)$$

When the superconductor is type I, the phase difference $\theta_1 - \theta_2$ is expected to be small or weakly depending on the magnetic field. This is because the width of wire in experiment[13] is 1-5×10^{-6} m and the coherence length of the type I superconductors is of the order of micrometers. The coherence length is comparable or larger than

L_c. Thus it is possible to observe the conductance oscillations.

When the superconductor is type II, the phase difference can described by

$$\theta_2 - \theta_1 = \int_{\boldsymbol{r}_1}^{\boldsymbol{r}_2} \mathrm{d}\,\boldsymbol{r}\nabla\theta(\boldsymbol{r}). \qquad (5.3)$$

By using the expression of the supercurrents in the Ginzburg-Landau theory

$$\boldsymbol{J}(\boldsymbol{r}) = en_s\left[\frac{\hbar}{2m_S}\nabla\theta(\boldsymbol{r}) + \frac{e}{m_S c}\boldsymbol{A}(\boldsymbol{r})\right], \qquad (5.4)$$

eq. (5.2) is estimated to be

$$F = \frac{2e}{\hbar c}\int_{\boldsymbol{r}_1}^{\boldsymbol{r}_2}\mathrm{d}\boldsymbol{r}_N\boldsymbol{A}(\boldsymbol{r}_N) - \frac{2e}{\hbar c}\int_{\boldsymbol{r}_1}^{\boldsymbol{r}_2}\mathrm{d}\boldsymbol{r}_S\boldsymbol{A}(\boldsymbol{r}_S)$$
$$-\frac{2m_S}{en_s\hbar}\int_{\boldsymbol{r}_1}^{\boldsymbol{r}_2}\mathrm{d}\boldsymbol{r}_S\boldsymbol{J}(\boldsymbol{r}_S), \qquad (5.5)$$

where n_s is the density of electrons and $\boldsymbol{r}_S$ is a dominant path of the supercurrents between $\boldsymbol{r}_1$ and $\boldsymbol{r}_2$ in the superconductor. First we consider the situation where the screened magnetic field is smaller than H_{c_1}. When the magnetic field is applied in the z direction, the supercurrents in the superconductor are calculated as

$$\boldsymbol{J} = \frac{cB}{4\pi\lambda}\mathrm{e}^{-\lambda x}\hat{\boldsymbol{y}}, \qquad (5.6)$$

where $\lambda = \sqrt{m_S c^2/4\pi n_s e^2}$ is the penetration depth in the superconductor. Here we solve eq. (5.4) with one of the Maxwell equation

$$\nabla \times \boldsymbol{B} = \frac{4\pi}{c}\boldsymbol{J}. \qquad (5.7)$$

The right hand side of eq. (5.5) can be rewritten

$$F = 4\pi\Phi/\phi_0 - \frac{2m_S}{en_s\hbar}\int_{y_1}^{y_2}\mathrm{d}y\,J_y, \qquad (5.8)$$

where Φ is the magnetic flux encircled by $\boldsymbol{r}_N$ and $\boldsymbol{r}_S$. Since the penetration depth is of the order of 10^{-7} m, the wire width is larger than the penetration depth and the supercurrents path is localized near the interface as shown in Fig. 9(a). The last term is independent of the magnetic field because the supercurrents are proportional to B and $y_1 - y_2$ is proportional to $1/B$. The conductance oscillations can be seen because the magnetic flux in the superconductor is much smaller than that in a semiconductor. Strictly speaking, the conductance is no longer periodic function of the inverse of the magnetic field because the magnetic flux in the superconductor is proportional to the magnetic field. When the screened magnetic field is larger than H_{c_1} as in the experiment, the supercurrents flows far from the interface as shown in Fig. 9(b) and the magnetic flux Φ depends on the supercurrents path and on the position of the vortices.[9] The conductance oscillations may be washed out since it is impossible to determine the dominant supercurrents path uniquely.

The conductance oscillations are sensitive to imperfections near the Sm-S interface, such as impurities, because a quasiparticle is diffused from the cyclotron orbit by the impurity scattering. In a recent paper, however, it is nu-
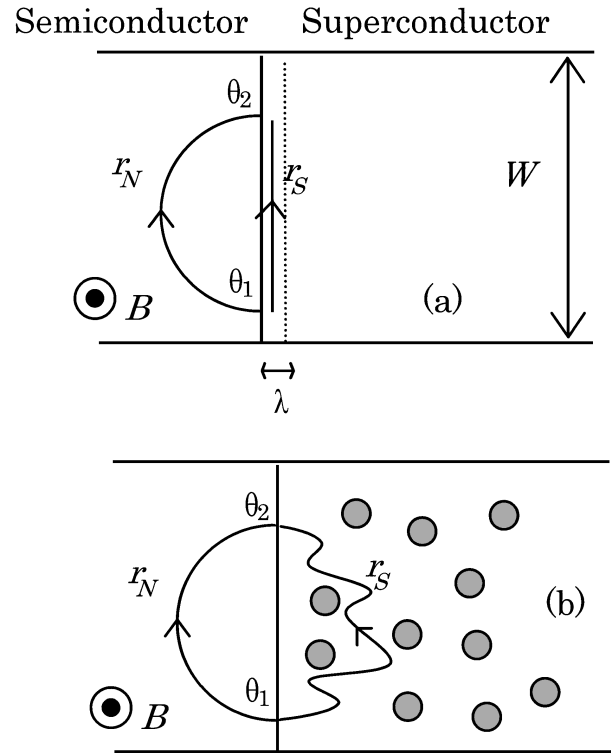

Fig. 9. The path of the supercurrents ($\boldsymbol{r}_S$) is illustrated when the magnetic field is smaller than H_{c_1} in (a). In (b), we draw one of the supercurrents paths when the magnetic field is larger than H_{c_1}. The gray circles in (b) denote the vortices.

merically shown that the conductance oscillations can be seen when the semiconductor near the interface is in the quasi-ballistic transport regime.[25] In addition to the imperfection in the 2DEG, the specular reflection at the Sm-S interface is an important ingredient to observe the conductance oscillations. In order to make clear the effects of disorder, a further study must be necessary. The investigation in this direction is now in progress and the results will be given elsewhere.[26]

§6. Conclusion

We have studied the magnetoconductance oscillations in small ballistic semiconductor-superconductor (Sm-S) junctions. These conductance oscillations were first shown in a previous numerical study.[17] However the mechanism of the oscillations has been unclear. In this paper, we reveal the nature of the magnetoconductance oscillations based on the phenomenology of the Aharonov-Bohm type interference effect. A possibility of observing the conductance oscillations is also discussed. The analytic expression of the conductance well explains the period, the amplitude and the phase shift of the conductance oscillations which are shown in the numerical simulation. We conclude that the interplay between the classical cyclotron motion of a quasiparticle and the interference effect due to the magnetic field is the origin of the magnetoconductance oscillations. Although there is no artificial confinement in the propagation path of a quasiparticle, the charge degree of freedom of an electron restricts an electron wave into the classical trajectory of the cyclotron motion under the magnetic field. In addi-

tion, the superconductor opens the hole conducting channels in the semiconductor. We show that the character of the Andreev reflection in magnetic field naturally leads to the Aharonov-Bohm type conductance oscillations in the simply connected Sm-S junctions.

Acknowledgements

Appendix: S-matrix in One-Dimensional Sm-S Junctions

In the appendix, we summarize the S-matrix in one-dimensional Sm-S junctions. The junction consists of a normal conductor ($x < 0$) and a superconductor ($x > 0$). The Bogoliubov-de Gennes equation reads,

$$\begin{pmatrix} H_0 & \Delta(x) \\ \Delta(x)^* & -H_0^* \end{pmatrix} \begin{pmatrix} u(x) \\ v(x) \end{pmatrix} = E \begin{pmatrix} u(x) \\ v(x) \end{pmatrix}, \quad (\text{A}\cdot1)$$

where $u(x)$ and $v(x)$ are the wavefunctions of a quasiparticle. The Hamiltonian is given by

$$H_0 = -\frac{\hbar^2}{2m^*}\frac{d^2}{dx^2} + H\delta(x) - \mu, \quad (\text{A}\cdot2)$$

where the mass of an electron m^* is m_N for $x \leq 0$ and m_S for $x > 0$, respectively. The chemical potential of the junction is denoted by μ. We set the chemical potential as an origin of the energy, (i.e., $\mu = 0$). The Fermi energy in a normal conductor is μ_N which corresponds to the energy difference between the band edge and the chemical potential. The Fermi energy in superconductor is μ_S. The potential barrier at the interface is described by $H\delta(x)$. The pair potential is given by the step function

$$\Delta(x) = \Theta(x)\Delta_0 e^{i\theta_S}, \quad (\text{A}\cdot3)$$

where θ_S is the phase of the pair potential. Since we focus on the zero-bias conductance in this paper, we estimate the S-matrix for $E = 0$. The wavefunction on either sides of the junction are described by

$$\hat{\Psi}^N(x) = a\begin{pmatrix} 1 \\ 0 \end{pmatrix} e^{ikx} + A\begin{pmatrix} 1 \\ 0 \end{pmatrix} e^{-ikx}$$

$$+b\begin{pmatrix} 0 \\ 1 \end{pmatrix} e^{-ikx} + B\begin{pmatrix} 0 \\ 1 \end{pmatrix} e^{ikx}, \quad (\text{A}\cdot4)$$

$$\hat{\Psi}^S(x) = C\begin{pmatrix} u_0 \\ v_0 e^{-i\theta_S} \end{pmatrix} e^{iqx} + D\begin{pmatrix} v_0 e^{i\theta_S} \\ u_0 \end{pmatrix} e^{-iqx}$$

$$+c\begin{pmatrix} u_0 \\ v_0 e^{-i\theta_S} \end{pmatrix} e^{-iqx} + d\begin{pmatrix} v_0 e^{i\theta_S} \\ u_0 \end{pmatrix} e^{iqx},$$

$$(\text{A}\cdot5)$$

with

$$k = \sqrt{\frac{2m_N\mu_N}{\hbar^2}}, \quad (\text{A}\cdot6)$$

$$q = \sqrt{\frac{2m_S}{\hbar^2}}(\mu_S^2 + \Delta_0^2)^{1/4}e^{i\delta/2}, \quad (\text{A}\cdot7)$$

$$\tan\delta = \frac{\Delta_0}{\mu_S}, \quad (\text{A}\cdot8)$$

$$u_0 = 1/\sqrt{2}, \quad (\text{A}\cdot9)$$

$$v_0 = -i/\sqrt{2}, \quad (\text{A}\cdot10)$$

where A, B, C and B denote the amplitudes of the outgoing waves from the interface, and a, b, c and d denote those of the incoming waves. The amplitudes of the outgoing waves are connected with those of the incoming waves by the continuity condition at $x = 0$,

$$\left[\hat{\Psi}^N - \hat{\Psi}^S\right]\Big|_{x=0} = 0, \quad (\text{A}\cdot11)$$

$$\frac{d}{dx}\left[\hat{\Psi}_n^N - \frac{m_N}{m_S}\hat{\Psi}_n^S\right]\Big|_{x=0} = -\frac{2m_N H}{\hbar^2}\hat{\Psi}^S\Big|_{x=0}. \quad (\text{A}\cdot12)$$

When $E = 0$, there is no propagating channel in the superconductor. Therefore an incoming quasiparticle from a normal conductor is alternatively reflected into the electron branch or the hole branch. The S-matrix in this case is reduced to a 2×2 matrix which connects (A, B) with (a, b),

$$\begin{pmatrix} A \\ B \end{pmatrix} = \begin{pmatrix} r_{ee} & r_{eh} \\ r_{he} & r_{hh} \end{pmatrix} \begin{pmatrix} a \\ b \end{pmatrix}, \quad (\text{A}\cdot13)$$

with

$$r_{ee} = \frac{\sqrt{(1 - |\xi|^2)^2 + (2\text{Im}\xi)^2}}{1 + |\xi|^2}e^{i\theta_n} \quad (\text{A}\cdot14)$$

$$r_{he} = 2\frac{\text{Re}\xi}{1 + |\xi|^2}e^{-i\pi/2}e^{-i\theta_S}, \quad (\text{A}\cdot15)$$

$$r_{hh} = \frac{\sqrt{(1 - |\xi|^2)^2 + (2\text{Im}\xi)^2}}{1 + |\xi|^2}e^{-i\theta_n}, \quad (\text{A}\cdot16)$$

$$r_{eh} = 2\frac{\text{Re}\xi}{1 + |\xi|^2}e^{-i\pi/2}e^{i\theta_S}, \quad (\text{A}\cdot17)$$

$$\xi = \frac{m_N}{m_S}\sqrt{\frac{2m_S}{\hbar^2 k^2}}(\mu_S^2 + \Delta_0^2)^{1/4}e^{i\delta/2} + iV_{bh}, \quad (\text{A}\cdot18)$$

$$V_{bh} = \frac{2m_N H}{\hbar^2 k}, \quad (\text{A}\cdot19)$$

$$\tan\theta_n = -\frac{2\text{Im}\xi}{1 - |\xi|^2}. \quad (\text{A}\cdot20)$$

Here θ_n is the phase shift of the normal reflection. In the limit of $\Delta_0 \ll \mu_N$, ξ and $\tan\theta_n$ are approximately estimated as

$$\xi \simeq \sqrt{\frac{m_N}{m_S}\frac{\mu_S}{\mu_N}} + iV_{bh} = \frac{v_F^S}{v_F^N} + iV_{bh} \quad (\text{A}\cdot21)$$

$$\tan\theta_n \simeq \frac{2V_{bh}}{\dfrac{m_N}{m_S}\dfrac{\mu_S}{\mu_N} - 1 + V_{bh}^2}, \quad (\text{A}\cdot22)$$

where v_F^S and v_F^N are the Fermi velocity in the superconductor and the semiconductor, respectively. As shown in eqs. (A·14), (A·16) and (A·21), the normal reflection coefficient becomes zero when $\xi = 1$. The condition is satisfied when $m_S/m_N = \mu_S/\mu_N$ and $V_{bh} = 0$.

1) R. A. Webb, S. Washburn, C. P. Umbach and R. B. Laibowitz: Phys. Rev. Lett. **54** (1985) 2696.
2) Y. Aharonov and D. Bohm: Phys. Rev. **115** (1959) 485.
3) H. van Houten, B. J. van Wees, J. E. Mooij, C. W. J. Beenakker, J. G. Williamson and C. T. Foxon: Europhys. Lett. **5** (1988) 721; H. van Houten, C. W. J. Beenakker, J. G. Williamson, M. E. I. Broekaart, P. H. M. van Loosdrecht, B. J. van Wees, J. E. Mooij, C. T. Foxon and J. J. Harris: Phys. Rev. B **39** (1989) 8556.
4) P. A. M. Benistant, H. van Kempen and P. Wyder: Phys. Rev. Lett. **51** (1983) 817.
5) C. W. J. Beenakker and H. van Houten: *Solid State Physics* **44** (Academic Press, New York, 1991), Chap. 4, and refereces there in.
6) B. J. van Wees and H. Takayanagi: *Mesoscopic Electron Transport*, ed. L. L. Sohn, L. P. Kouwenhoven and G. Schön, NATO ASI Series, (Kluwer Academic, Dordrecht, 1996).
7) C. W. J. Beenakker: Rev. Mod. Phys. **69** (1997) 731, and references there in.
8) A. F. Morpurgo, S. Holl, B. J. van Wees, T. M. Klapwijk and G. Borghs: Phys. Rev. Lett. **78** (1997) 2636.
9) F. W. J. Hekking and Yu. V. Nazarov: Phys. Rev. Lett. **71** (1993) 1625.
10) G. Bastian, E. O. Göbel, A. B. Zorin, H. Schlze, J. Niemeyer, T. Weimann, M. R. Benett and K. E. Singer: Phys. Rev. Lett. **81** (1998) 1686.
11) A. F. Andreev: Zh. Eksp. Theor. Fiz, **46** (1964) 1823. *ibid.* Sov. Phys. JETP **19** (1964) 1228.
12) G. E. Blonder, M. Tinkham and T. M. Klapwijk: Phys. Rev. B **25** (1982) 4515.
13) H. Takayanagi and T. Akazaki: Physica B **249**–**251** (1998) 462.
14) T. D. Moore and D. A. Williams, Phys. Rev. B **59** (1999) 7308.
15) A. Yu. Zyuzin: Phys. Rev. B **50** (1994) 323.
16) Y. Ishikawa and H. Fukuyama: J. Phys. Soc. Jpn. **68** (1999) 954.
17) Y. Takagaki: Phys. Rev. B **57** (1998) 4009.
18) Y. Asano: Phys. Rev. B **61** (2000) 1732.
19) P. G. de Gennes: *Superconductivity of Metals and Alloys* (Benjamin, New York, 1996).
20) U. Schüssler and R. Kümmel: Phys. Rev. B **47** (1993) 2754.
21) H. Tamura and T. Ando: Phys. Rev. B **44** (1991) 1792.
22) Y. Takane and H. Ebisawa: J. Phys. Soc. Jpn. **61** (1992) 1685.
23) H. Hoppe, U. Zülicke and G. Schön: Phys. Rev. Lett. **84** (2000) 1804.
24) M. J. M. de Jong and C. W. J. Beenakker: Phys. Rev. Lett. **74** (1995) 1657.
25) Y. Takagaki and K. H. Ploog: Phys. Rev. B **58** (1998) 7162.
26) Y. Asano and T. Yuito: in preparation.